Journal of Computational Physics 229 (2010) 2550–2572

Contents lists available at ScienceDirect

Journal of Computational Physics

journal homepage: www.elsevier.com/locate/jcp

Symplectic wavelet collocation method for Hamiltonian wave equations

Huajun Zhu [a,*], Lingyan Tang [a], Songhe Song [a], Yifa Tang [b], Desheng Wang [c]

[a] Department of Mathematics and System Science, Science School, National University of Defense Technology, Changsha, Hunan 410073, China
[b] LSEC, ICMSEC, Academy of Mathematics and Systems Science, Chinese Academy of Science, P.O. Box 2719, Beijing 100190, China
[c] Division of Mathematical Sciences, School of Physical and Mathematical Sciences, Nanyang Technological University, Singapore 637371, Singapore

ARTICLE INFO

Article history:
Received 30 June 2009
Received in revised form 28 November 2009
Accepted 30 November 2009
Available online 11 December 2009

Keywords:
Wavelet collocation
Symplectic scheme
Hamiltonian system

ABSTRACT

This paper introduces a novel symplectic wavelet collocation method for solving nonlinear Hamiltonian wave equations. Based on the autocorrelation functions of Daubechies compactly supported scaling functions, collocation method is conducted for the spatial discretization, which leads to a finite-dimensional Hamiltonian system. Then, appropriate symplectic scheme is employed for the integration of the Hamiltonian system. Under the hypothesis of periodicity, the properties of the resulted space differentiation matrix are analyzed in detail. Conservation of energy and momentum is also investigated. Various numerical experiments show the effectiveness of the proposed method.

1. Introduction

Due to the symplectic geometric structures, Hamiltonian systems are useful for modeling physical process with negligible dissipative effects and have been applied to various fields involving weather prediction, nonlinear optics, oceanography and quantum field theory and so on. It is of much significance to preserve the intrinsic properties of the original problem during numerical simulations, i.e. to preserve the symplectic geometric structure of the Hamiltonian system. And various symplectic approaches have been developed [4,6,7,11,13,15,16,23,24,31]. One standard method to obtain symplectic method for an infinite-dimensional Hamiltonian PDE is that, first discretize the Hamiltonian PDE in space to obtain a finite-dimensional Hamiltonian system, and then evolve the semi-discrete system in time by symplectic integrators [27,28]. In this numerical procedure, the key for success is to ensure that the obtained semi-discrete system is a finite-dimensional Hamiltonian ODE system, for which finite difference method (FDM) [6], finite element method (FEM) [33], Fourier pseudospectral method [14] can be utilized, but not well for singular problems [20]. To develop an effective and robust numerical method for the space discretization of a Hamiltonian system whose solution is of singularity or sharp transition motivates the current work.

Wavelet-based numerical methods have gained popularity as they take the advantages of both spectral method and FDM (or FEM), which makes the methods very attractive for solving singular problems (see [19–22,25]). Compared with FDM and FEM, wavelet-based methods can have higher order of accuracy, and compared with spectral method, wavelet-based methods have good spatial localization and generate a sparse space differentiation matrix. The wavelet-based algorithms can be roughly classified into two categories: wavelet-Galerkin and wavelet collocation, which can been utilized to construct symplectic algorithms. In [11] and [12], Daubechies' compactly supported orthogonal wavelets and second-generation wavelets are proposed to combine with symplectic schemes to construct multiresolution symplectic solvers for wave propagation problems and the method is of wavelet-Galerkin type. However, the two papers lack theoretical analysis and numerical simulations. And, following the proposed method, it is very difficult to deal with nonlinearities, as it needs the passage between the wavelet space and physical space, which is not cost-effective in computations.

* Corresponding author. Tel.: +86 13974958901.
E-mail address: girl–zhu@163.com (H. Zhu).

0021-9991/$ - see front matter © 2009 Elsevier Inc. All rights reserved.
doi:10.1016/j.jcp.2009.11.042

To address the above issues, symplectic wavelet collocation method (abbr. SWCM) is proposed for Hamiltonian wave equations in this paper. Nonlinear wave (NLW) equation and nonlinear Schrödinger (NLS) equation are tested. The main contributions of the work go as follows:

1. The wavelet collocation method is applied for the first time to construct symplectic schemes. The collocation method is based on the autocorrelation functions of Daubechies compactly supported scaling functions. After discretizing spatially by the wavelet collocation method, we have obtained a semi-discrete finite-dimensional Hamiltonian system, which is proved theoretically. Symplectic Runge–Kutta methods are then used for the time integration. The autocorrelation function initially proposed in [25] has the merits of symmetry and nice interpolation properties, which leads to that the interpolation coefficients are exactly the numerical solutions at collocation points. Hence no additional computation is required for the determination of the passage between the wavelet and physical space, which renders the whole procedure very efficient.
2. Under the hypothesis of regularity and periodicity, the properties of space differentiation matrix are investigated in detail, which is very useful for analyzing the performance of the proposed method. Furthermore, the convergence of the proposed method is proved theoretically and it is concluded that the method is of high order of accuracy in space. Based on the nice properties of the space differentiation matrix, conservation of invariants is also investigated.
3. Various numerical experiments for the NLW and NLS equations are conducted to substantiate the theoretical results. All the experimental results show that the developed symplectic method captures singularities very well. In addition, the method has exponential convergence rate in space. When the support interval of the autocorrelation function becomes larger, the method will possesses similar accuracy with pseudospectral method. However, the SWCM demands less computations because of the sparseness of the space differentiation matrix, which has been numerically proved as well. The numerical results show that SWCM takes a good balance of accuracy and efficiency. Finally, the data statistics of the errors of invariants demonstrate our theoretical analysis very well.

The rest of the paper is organized as follows. In Section 2, preliminaries about the nonlinear wave equation and its discretization methods are recalled. Autocorrelation functions and their interpolation operators are also presented. In Section 3, SWCM is introduced and the properties of the space differentiation matrix are discussed in detail. The convergence property and conservation of Hamiltonian and momentum are also analyzed. In Section 4, SWCM is generalized to NLS equation. In Section 5, numerical experiments for NLW and NLS equations with symmetric and nonsymmetric initial conditions are conducted to illustrate the effectiveness of the method. Finally, concluding remarks are given in Section 6.

2. Preliminaries about the nonlinear wave equation and wavelet

2.1. Nonlinear wave equation

We consider the nonlinear wave equation with periodic boundary condition

$$u_{tt} = u_{xx} - F'(u), \quad u(a,t) = u(b,t), \quad x \in [a,b],\ t \in [0,T], \tag{1}$$

where $F : R \to R$ is a smooth function. The equation is used to model nonlinear phenomena such as the propagation of dislocations in crystals and the behavior of elementary particles. It is also used in soliton theory. The equation is a classical example of Hamiltonian PDEs. The Hamiltonian formulation goes as

$$\begin{cases} u_t = v, \\ v_t = u_{xx} - F'(u) \end{cases} \tag{2}$$

for which the Hamiltonian

$$H(u,v) = \frac{1}{2}\int \left[v^2 + u_x^2 + 2F(u)\right] dx \tag{3}$$

and momentum

$$M = -\int u_t u_x \, dx \tag{4}$$

are invariant with respect to time.

2.2. Discretization method for the NLW equation

To solve (2) numerically, a standard solution procedure starts with the discretization of the equation in space and then does the time integration. The spatial discretization results in the following semi-discrete system

$$\begin{cases} \frac{dU_h(t)}{dt} = V_h(t), \\ \frac{dV_h(t)}{dt} = A_h U_h(t) - F'(U_h(t)), \end{cases} \tag{5}$$

where h is the space step, $U_h(t)$ and $V_h(t)$ are the approximate solutions at time t. In order to preserve the symplectic form of (2), an appropriate numerical discretization scheme needs to be developed in the sense that the above resulting semi-discrete system (continuous in time) can be written as a finite-dimensional Hamiltonian system. For this purpose, the numerical scheme is required to be able to preserve the symmetric property of second-order differential operator embedded in (2). Several methods can be chosen such as the finite difference method (FDM), finite element method (FEM) and Fourier pseudospectral method.

The Fourier pseudospectral method can lead to a symmetric spectral differentiation matrix with high accuracy [14], which is a full matrix and normally requires expensive computations. However, the differentiation matrix obtained by a suitable choice of wavelets is symmetric and sparse. The wavelet-based method has some advantages over the traditional FDM, FEM and spectral method [11,12] while there are no theoretical analysis and numerical simulations, which renders the readers unsure about the effectiveness of the method.

In this paper, a wavelet collocation method will be used for the spatial discretization of the Hamiltonian wave equation for the first time. The autocorrelation functions of Daubechies scaling functions will be used as trial functions, which make the second-order differentiation matrix be symmetric and sparse. The resulting spatial discretization is a good balance of accuracy (Fourier pseudospectral method) and efficiency (FDM or FEM). The details of the proposed wavelet collocation method will be given in Section 3 next, before which the properties of autocorrelation functions and the interpolation operator are presented in the following.

2.3. Wavelet and multiresolution

A Daubechies scaling function $\phi(x)$ of order M (in short, DM) satisfies the scaling relation:

$$\phi(x) = \sum_{k=0}^{M-1} h_k \phi(2x-k), \tag{6}$$

where M is a positive even integer and $\{h_k\}_{k=0}^{M-1}$ are M non-vanishing "filter coefficients". The function has its support in the interval $[0, M-1]$ and it has $(M/2-1)$ vanishing wavelet moments. Furthermore, a multiresolution analysis can be conducted on $L^2(R)$ [10].

Define the autocorrelation function $\theta(x)$ of $\phi(x)$ (in short, ADM) as

$$\theta(x) = (\phi * \phi(-\cdot))(x) = \int \phi(x)\phi(t-x)\,dt. \tag{7}$$

Suppose that V_j is the linear span of $\{\theta_{j,k}(x) = 2^{j/2}\theta(2^j x - k),\ k \in Z\}$, then it can be proved that $(V_j)_{j\in Z}$ forms a multiresolution analysis where $\theta(x)$ plays the role of scaling function. The function $\theta(x)$ has nice properties as follows:

1. Compactly supported:
$$supp(\theta(x)) = [-M+1, M-1]. \tag{8}$$
2. Interpolation property:
$$\theta(l) = \int \phi(x)\phi(x-l)\,dx = \delta_{0,l}, \quad l \in Z. \tag{9}$$
3. Derivative property: the odd-order derivative of $\theta(x)$ is an odd function, and the even-order derivative of $\theta(x)$ is an even function, i.e.
$$\theta^{2k}(-x) = \theta^{2k}(x), \quad \theta^{2k+1}(-x) = -\theta^{2k+1}(x), \quad l = 0, 1, 2, \ldots \tag{10}$$
4. Scaling property: the autocorrelation coefficients of the filter $H = \{h_k\}_{k=1}^{M-1}$ are
$$c_k = 2\sum_{l=0}^{M-1-k} h_l h_{l+k}, \quad k = 1, \ldots, M-1 \tag{11}$$
and
$$c_{2k} = 0, \quad k = 1, \ldots, M/2-1, \tag{12}$$
based on which a scaling relation similar to (6) [1,9] can be derived as
$$\theta(x) = \theta(2x) + \frac{1}{2}\sum_{l=1}^{M/2} c_{2l-1}(\theta(2x-2l+1) + \theta(2x+2l-1)). \tag{13}$$

There is no analytical expression for $\theta^{(k)}(x)$ $(k = 0, 1, 2, \ldots)$, but the values at dyadic points can be computed up to the machine precision. The values of the function $\theta^{(k)}(x)$ at integer points $x = l$ $(l = 0, \pm 1, \ldots, \pm(M-1))$ can be obtained by solving an eigenvalue problem which is derived from the scaling relation (13) [1,21]. Then, the values of $\theta^{(k)}(x)$ $(k = 0, 1, 2, \ldots)$ at

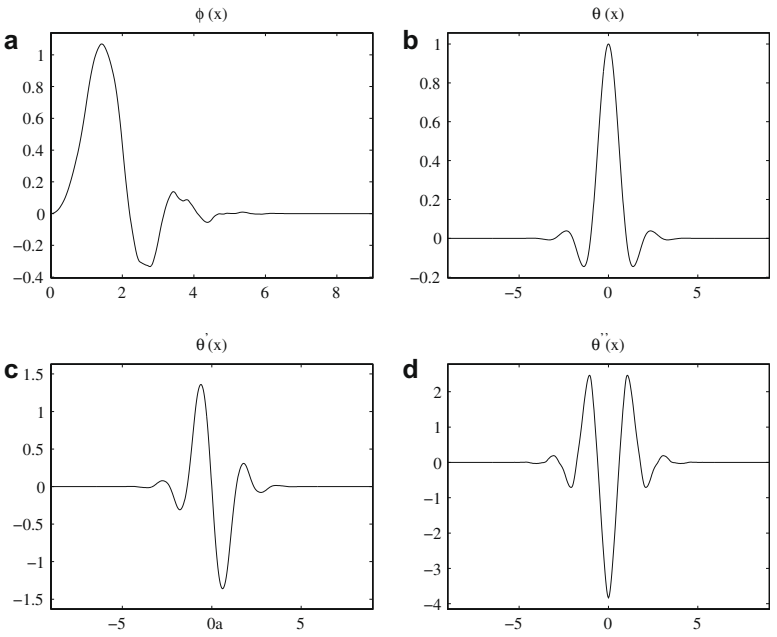

Fig. 1. (a) Daubechies scaling function D10, (b) its autocorrelation function θ, (c) first derivative θ' and (d) second derivative θ''.

dyadic points can be computed recursively from the values at integer points using the matrix method [10,21]. For illustrations, the scaling function and its autocorrelation function of D10 are shown in Fig. 1.

Define an interpolation operator on V_j (with the space step $h = 2^{-j}$) as

$$I_j u(x) = 2^{-\frac{j}{2}} \sum_k u(2^{-j}k)\theta_{j,k}(x) = \sum_k u(2^{-j}k)\theta(2^j x - k), \tag{14}$$

then the following estimate on the interpolation error holds [25].

Lemma 2.1. *Let* $0 \leqslant r \leqslant s \leqslant 2M-1,\ s \geqslant 1$, *and* $u \in H^s(R)$, *then*

$$\|u - I_j u\|_r \leqslant C 2^{-j(s-r)} \|u\|_s, \tag{15}$$

where $\|\cdot\|_r$ *and* $\|\cdot\|_s$ *denote the norm of Sobolev space* $H^r(R)$ *and* $H^s(R)$, *respectively.*

3. Symplectic wavelet collocation method for the NLW equation

3.1. Symplectic wavelet collocation method

Wavelet collocation method is used for space discretization which result in a finite-dimensional Hamiltonian system. The Hamiltonian system is then integrated in time by symplectic methods.

3.1.1. Wavelet collocation method for space discretization

In this section, a wavelet collocation method, which is based on the autocorrelation function $\theta(x)$ of the compactly supported Daubechies scaling functions, is used for space discretization, and the discretized system is proved to be a Hamiltonian system under periodic boundary conditions.

Consider the NLW equation (2) with the spatial domain being $[a, b]$, where a and b are integers. We use the autocorrelation function $\theta(x)$ of Daubechies scaling function DM in the framework of a collocation method. Taking a fixed scale $J =$ constant, we approximate $u(x,t)$ and $v(x,t)$ by interpolation operators $I_J u(x,t)$ and $I_J v(x,t)$ on V_J, respectively, which interpolate $u(x,t)$ and $v(x,t)$ at collocation points $x_m = a + m/2^J$, for $m = 0, 1, \ldots, N-1,\ N = (b-a)\cdot 2^J$. The interpolation operators $I_J u(x,t)$ and $I_J v(x,t)$ have the form

$$u_J(x,t) = I_J u(x,t) = \sum_{m=0}^{N-1} u(x_m,t)\theta(2^J x - (a\cdot 2^J + m)), \tag{16}$$

$$v_J(x,t) = I_J v(x,t) = \sum_{m=0}^{N-1} v(x_m,t)\theta(2^J x - (a\cdot 2^J + m)). \tag{17}$$

According to the interpolating property of $\theta(x)$ (9), we have

$$u_J(x_m,t)=u(x_m,t),\ v_J(x_m,t)=v(x_m,t).$$

Applying the wavelet collocation method for the space discretization of system (2), we obtain

$$\begin{cases}(u_J(x_m,t))_t=v_J(x_m,t),\\(v_J(x_m,t))_t=(u_J(x,t))_{xx}|_{x=x_m}-F'(u_J(x_m,t)).\end{cases}\tag{18}$$

To obtain the equations for $u_J(x_m,t)$ and $v_J(x_m,t)$, the crucial step is to express the kth-order spatial partial derivatives $\left\{\frac{\partial^k u_J(x,t)}{\partial x^k}\right\}$ at collocation points x_m in terms of the values $u_J(x_m,t)$. This is done by making k-times differential with (16) and evaluating the resulting expressions at collocation points x_m:

$$\left.\frac{\partial^k u_J(x,t)}{\partial x^k}\right|_{x_m}=\sum_{m'=0}^{N-1}u(x_{m'},t)\cdot\left.\frac{d^k\theta(2^Jx-m')}{dx^k}\right|_{x_m}=(B_kU_J)_m,\tag{19}$$

where B_k is a $N\times N$ matrix with elements

$$(B_k)_{m,m'}=\left.\frac{d^k\theta(2^Jx-m')}{dx^k}\right|_{x_m}=2^{kJ}\theta^{(k)}(m-m')$$

and $U_J=(u_J(x_0,t),u_J(x_1,t),\ldots,u_J(x_{N-1},t))^T$.

Now, we investigate the properties of the space differentiation matrix B_k. Since $\theta(x)$ is locally supported within the interval $[-M+1,M-1]$, we have that $(B_k)_{m,m'}=0$ for $m'<m-M+1$ and $m'>m+M-1$. Considering periodic boundary conditions, the space differentiation matrix B_k can be expressed as

$$(B_k)_{m,m'}=\begin{cases}2^{kJ}\theta^{(k)}(m-m'), & m-(M-1)\leqslant m'\leqslant m+(M-1);\\ 2^{kJ}\theta^{(k)}(-l), & m-m'=N-l,\ 1\leqslant l\leqslant M-1;\\ 2^{kJ}\theta^{(k)}(l), & m'-m=N-l,\ 1\leqslant l\leqslant M-1;\\ 0, & \text{otherwise}.\end{cases}\tag{20}$$

Obviously, B_k is a $N\times N$ sparse matrix with $(2M-1)$ nonzero elements in each row, and we have

$$(B_kU_J)_m=\sum_{m'=m-M+1}^{m+M-1}u_J(x_{m'})2^{kJ}\theta^{(k)}(m-m').$$

In particular for the autocorrelation function of D4, the matrix B_k can be expressed as

$$B_k=2^{kJ}\begin{pmatrix}b_0&b_{-1}&b_{-2}&b_{-3}&&&b_3&b_2&b_1\\ b_1&b_0&b_{-1}&b_{-2}&b_{-3}&&&b_3&b_2\\ b_2&b_1&b_0&b_{-1}&b_{-2}&b_{-3}&&&b_3\\ b_3&b_2&b_1&b_0&b_{-1}&b_{-2}&b_{-3}&&\\ &&&&\ddots&&&&\\ &&b_3&b_2&b_1&b_0&b_{-1}&b_{-2}&b_{-3}\\ b_{-3}&&&b_3&b_2&b_1&b_0&b_{-1}&b_{-2}\\ b_{-2}&b_{-3}&&&b_3&b_2&b_1&b_0&b_{-1}\\ b_{-1}&b_{-2}&b_{-3}&&&b_3&b_2&b_1&b_0\end{pmatrix},$$

where $b_l=\theta^{(k)}(l)$ and l is an integer in $-3\leqslant l\leqslant 3$. The properties of B_k are presented in detail in the following theorem.

Theorem 3.1. *For the autocorrelation function of Daubechies scaling function DM, the space differentiation matrix B_k in (19) has the following properties:*

(1) *B_{2k} is symmetric, and B_{2k+1} is antisymmetric.*
(2) *B_k is a circulant matrix with bandwidth of $2M-1$, and $B_{2k}B_{2k'+1}$ is a antisymmetric circulant matrix with a bandwidth of $4M-3$. Recursively, $B_{2k}B_{2k'}$ and $B_{2k+1}B_{2k'+1}$ are symmetric circulant matrixes with bandwidth of $4M-3$.*
(3) *The eigenvalues of circulant matrix B_k are*

$$\lambda_j=\hat\theta^{(k)}(\omega_j),\quad \omega_j=-\frac{2\pi}{N}j,\ j=0,1,\ldots,N-1,$$

where $\hat\theta^{(k)}(\omega)$ is the Fourier transform of $\theta^{(k)}(x)$. And the following equality holds

$$FB_kF^*=diag(\hat\theta^{(k)}(\omega_0),\hat\theta^{(k)}(\omega_1),\ldots,\hat\theta^{(k)}(\omega_{N-1})),$$

where F^* is the Fourier matrix.
(4) *B_{4k+2} is negative semidefinite, and B_{4k} is positive semidefinite.*

Proof

(1) Because $\theta^{(2k)}(-x)=\theta^{(2k)}(x)$ and $\theta^{(2k+1)}(-x)=-\theta^{(2k+1)}(x)$, we have

$$(B_{2k})_{m',m}=2^{2kJ}\theta^{(2k)}(m'-m)=2^{2kJ}\theta^{(2k)}(m-m')=(B_{2k})_{m,m'},\quad m-(M-1)\leqslant m'\leqslant m+(M-1)$$

and

$$(B_{2k})_{m',m}=2^{2kJ}\theta^{(2k)}(-l)=2^{2kJ}\theta^{(2k)}(l)=(B_{2k})_{m,m'},\quad m-m'=N-l,1\leqslant l\leqslant M-1,$$

which shows that B_{2k} is a symmetric matrix. Similarly, it can be proved that B_{2k+1} is an antisymmetric matrix.

(2) Denote the first row of the matrix $2^{-kJ}B_k$ as

$$(c_0,c_1,\ldots,c_{N-1})=(\theta^{(k)}(0),\theta^{(k)}(-1),\ldots,\theta^{(k)}(-(M-1)),0,\ldots,0,\theta^{(k)}(M-1),\ldots,\theta^{(k)}(1)),$$

from which it can be concluded that B_k is a circulant matrix and $B_k=2^{kJ}\cdot Circ(c_0,c_1,\ldots,c_{N-1})$. Obviously, the bandwidth of B_k is $2M-1$. Let $B_{2k}=(a_{ij})$, $B_{2k'+1}=(b_{ij})$ and $C=B_{2k}B_{2k'+1}=(c_{ij})$, and we consider the items $\{c_{ij}|M-1<i,j<N-(M-1)\}$ in C. Since B_{2k} and $B_{2k'+1}$ have the same bandwidth of $2M-1$, then $c_{ij}=0$ for $|i-j|>2M-2$. Suppose $i>j$, we have

$$c_{ij}=\sum_{m=1}^{N}a_{im}b_{mj}=\sum_{m=i-(M-1)}^{j+M-1}2^{J(2k+2k'+1)}\theta^{(2l)}(i-m)\theta^{(2k'+1)}(m-j)=\sum_{r=-(M-1)}^{j-i+M-1}2^{J(2k+2k'+1)}\theta^{(2l)}(-r)\theta^{(2k'+1)}(r+i-j)$$

and

$$c_{ji}=\sum_{m=1}^{N}a_{jm}b_{mi}=\sum_{m=i-(M-1)}^{j+M-1}2^{J(2k+2k'+1)}\theta^{(2k)}(j-m)\theta^{(2k'+1)}(m-i)=-\sum_{r=-(M-1)}^{j-i+M-1}2^{J(2k+2k'+1)}\theta^{(2k)}(-r)\theta^{(2k'+1)}(r+i-j)=-c_{ij}.$$

In the same way, it can be proved that $c_{ji}=-c_{ij}$ for $i,j\geqslant N-(M-1)$ and $i,j\leqslant M-1$. Thus, C is antisymmetric. Moreover, we have

$$\begin{aligned}c_{i,2i-j}&=-c_{2i-j,i}=-\sum_{r=-(M-1)}^{i-(2i-j)+M-1}2^{J(2k+2k'+1)}\theta^{(2k)}(-r)\theta^{(2k'+1)}(r+(2i-j)-i)\\&=-\sum_{r=-(M-1)}^{i-(2i-j)+M-1}2^{J(2k+2k'+1)}\theta^{(2k)}(-r)\theta^{(2k'+1)}(r+(2i-j)-i)=-c_{i,j}.\end{aligned}$$

Therefore, $B_{2k}B_{2k'+1}$ is an antisymmetric circulant matrix with a bandwidth of $2(2M-2)+1$.Similarly, $B_{2k}B_{2k'}$ and $B_{2k+1}B_{2k'+1}$ are symmetric circulant matrices with bandwidth of $4M-3$.

(3) Suppose $B_k=2^{kJ}C$, $C=Circ(c_0,c_1,\ldots,c_{N-1})$, then there exists a Fourier matrix F^* [17] such that

$$FCF^*=diag(f_C(\zeta^0),f_C(\zeta^1),\ldots,f_C(\zeta^{N-1})),$$

where $f_C(x)=c_0+c_1x+\cdots+c_{N-1}x^{N-1}$, $\zeta=e^{\frac{2\pi}{N}i}$ $(i=\sqrt{-1})$, and

$$F^*=\frac{1}{\sqrt{N}}\begin{pmatrix}1&1&1&\cdots&1\\1&\zeta&\zeta^2&\cdots&\zeta^{N-1}\\1&\zeta^2&\zeta^4&\cdots&\zeta^{2(N-1)}\\\cdots&\cdots&\cdots&\cdots&\cdots\\1&\zeta^{N-1}&\zeta^{2(N-1)}&\cdots&\zeta^{(N-1)(N-1)}\end{pmatrix}.$$

Now consider the spectrum $SpecC=(f_C(\zeta^j))$. Because $\zeta^N=1$, we obtain

$$\lambda_j(C)=f_C(\zeta^j)=c_0+c_1(\zeta^j)+\cdots+c_{N-1}(\zeta^j)^{N-1}=\theta^{(k)}(0)+\sum_{r=1}^{M-1}\theta^{(k)}(-r)(\zeta^j)^r+\sum_{r=1}^{M-1}\theta^{(k)}(r)(\zeta^j)^{(N-r)}=\sum_{r=-(M-1)}^{M-1}\theta^{(k)}(r)(\zeta^j)^{-r}.$$

In addition, $\hat{\theta}^{(k)}(\omega)$, the Fourier transform of $\theta^{(k)}(x)$ [8], can be expressed as

$$\hat{\theta}^{(k)}(\omega)=\sum_{n\in\mathbb{Z}}|\hat{\varphi}(\omega+2\pi n)|^2(-i)^k(\omega+2\pi n)^k,$$

which can be written as

$$\hat{\theta}^{(k)}(\omega)=\sum_r\theta^{(k)}(r)e^{ir\omega}.$$

Thus,

$$\lambda_j(C)=\sum_{r=-(M-1)}^{M-1}\theta^{(k)}(r)(\zeta^j)^{-r}=\sum_{r=-(M-1)}^{M-1}\theta^{(k)}(r)\left(e^{\frac{2\pi}{N}i}\right)^{-jr}=\sum_{r=-(M-1)}^{M-1}\theta^{(k)}(r)e^{ir\left(-j\frac{2\pi}{N}\right)}=\hat{\theta}^{(k)}\left(-j\frac{2\pi}{N}\right).$$

Therefore,

$$\lambda_j(B_k)=2^{kJ}\hat{\theta}^{(k)}(\omega_j),\quad \omega_j=-j\frac{2\pi}{N},\ j=0,1,\ldots,N-1.$$

(4) First, for λ_0 we get

$$\lambda_0(2^{-kJ}B_k)=\hat{\theta}^{(k)}(0)=\sum_r\theta^{(k)}(r)=0.$$

Then, consider the other eigenvalues λ_j, for $j=1,\ldots,N-1$.For B_{4k+2}, we have

$$\lambda_j(2^{-(4k+2)J}B_{4k+2})=\hat{\theta}^{(4k+2)}(\omega_j)=\sum_{n\in\mathbb{Z}}|\hat{\varphi}(\omega_j+2\pi n)|^2(-i)^{4k+2}(\omega_j+2\pi n)^{4k+2}=\sum_{n\in\mathbb{Z}}|\hat{\varphi}(\omega_j+2\pi n)|^2(-1)(\omega_j+2\pi n)^{4k+2}<0.$$

Therefore, B_{4k+2} is negative semidefinite.Similarly, for B_{4k}, we have

$$\lambda_j(2^{-4kJ}B_{4k})=\hat{\theta}^{(4k)}(\omega_j)=\sum_{n\in\mathbb{Z}}|\hat{\varphi}(\omega_j+2\pi n)|^2(-i)^{4k}(\omega_j+2\pi n)^{4k}=\sum_{n\in\mathbb{Z}}|\hat{\varphi}(\omega_j+2\pi n)|^2\cdot 1\cdot(\omega_j+2\pi n)^{4k}>0.$$

Therefore, B_{4k} is positive semidefinite. This completes the proof of Theorem 3.1. □

Combining (18) with the differentiation matrix B_2, we arrive at the wavelet collocation semi-discretization for the nonlinear wave equation (2)

$$\begin{cases}\frac{d}{dt}u_J(x_m,t)=v_J(x_m,t),\\ \frac{d}{dt}v_J(x_m,t)=(B_2U_J)_m-F'(u_J(x_m,t)),\end{cases}\tag{21}$$

where $m=0,1,\ldots,N-1,\ U_J=(u_J(x_0,t),u_J(x_1,t),\ldots,u_J(x_{N-1},t))^T$. Note that the unknowns $u_J(x_m,t)$ and $v_J(x_m,t)$ in (21) are exactly the values of the approximate solution at the collocation points and no extra computation is required for the determination of the passage between wavelet coefficients and physical space.

Since B_2 is symmetric, the semi-discrete system (21) is a finite-dimensional Hamiltonian system [3,26]. Let $Z=(U_J,V_J)^T,\ J=\begin{bmatrix}0 & I_N\\ -I_N & 0\end{bmatrix}$, then (21) can be rewritten as

$$Z_t=J\nabla_Z H(Z)\tag{22}$$

with the Hamiltonian

$$H(U_J,V_J)=\frac{1}{2}\langle V_J,V_J\rangle+\langle F(U_J),\mathbf{1}\rangle-\frac{1}{2}\langle U_J,B_2U_J\rangle,\tag{23}$$

where $\langle\cdot,\cdot\rangle$ is the standard inner product.

The Hamiltonian system (22) satisfies the semi-discrete symplectic conservation law

$$\frac{d}{dt}\sum_{m=0}^{N-1}du_J(x_m,t)\wedge dv_J(x_m,t)=0,$$

where $\wedge$ is the wedge product.

3.1.2. Symplectic methods for time discretization

The semi-discrete finite-dimensional Hamiltonian system (22) can be discretized in time by lots of symplectic methods, such as generating function methods, Runge–Kutta methods, composition methods [18,24], and explicit symplectic schemes for separable Hamiltonian systems. Here we consider Runge–Kutta methods. By noting $f(Z)=J\nabla_Z H(Z)$, a symplectic Runge–Kutta method for the system (22) with s stage variables $\{K_l\}$ and coefficients $\{a_{lm}\},\ \{b_l\}$, can be written as

$$\begin{cases}K_l=Z^n+\tau\cdot\sum_{m=1}^{s}a_{lm}f(K_m),\\ Z^{n+1}=Z^n+\tau\cdot\sum_{l=1}^{s}b_lf(K_l),\end{cases}\qquad 1\leqslant l\leqslant s,$$

where τ is the time-step. When $s=1,\ a_{11}=1/2,\ b_1=1$, we have

$$Z^{n+1}=Z^n+\tau\cdot J\nabla_Z H\left(\frac{Z^n+Z^{n+1}}{2}\right),$$

which leads to the Euler-centered scheme in time, which is also known as the implicit midpoint scheme. In this paper, we use this scheme for time discretization.

Integrating the semi-discrete system (21) in time by the Euler-centered scheme, we obtain a symplectic wavelet collocation method for the NLW equation (1):

$$\begin{cases} U_J^{n+1} = U_J^n + \tau \cdot \frac{V_J^n + V_J^{n+1}}{2}, \\ V_J^{n+1} = V_J^n + \tau \cdot \left(B_2 \cdot \frac{U_J^n + U_J^{n+1}}{2} - F'\left(\frac{U_J^n + U_J^{n+1}}{2}\right)\right). \end{cases} \tag{24}$$

Suppose $\left(U_J^n, V_J^n\right)$ are given. We first solve the following equation for V_J^{n+1},

$$V_J^{n+1} = V_J^n + \tau \cdot \left(B_2 \cdot \left(U_J^n + \tau \cdot \frac{V_J^n + V_J^{n+1}}{4}\right) - F'\left(U_J^n + \tau \cdot \frac{V_J^n + V_J^{n+1}}{4}\right)\right), \tag{25}$$

then U_J^{n+1} are obtained as

$$U_J^{n+1} = U_J^n + \tau \cdot \frac{V_J^n + V_J^{n+1}}{2}. \tag{26}$$

Remark. The SWCM (24) is equivalent to the following scheme by eliminating the value V_J,

$$\frac{U_J^{n+1} - 2U_J^n + U_J^{n-1}}{\tau^2} = B_2\left(\frac{U_J^{n+1} + 2U_J^n + U_J^{n-1}}{4}\right) - \frac{1}{2}\left(F'\left(\frac{U_J^{n+1} + U_J^n}{2}\right) + F'\left(\frac{U_J^{n-1} + U_J^n}{2}\right)\right). \tag{27}$$

Although the SWCM (24) or (27) is an implicit scheme, the space differentiation matrix is sparse and iteration methods can be used in solving, such as *Newton Successive Over Relaxation Method* (N-SOR) and fixed-point iteration method, which render the proposed SWCM much efficient.

3.2. Theoretical analysis for SWCM

3.2.1. Convergence of SWCM

In this paper, our analysis is restricted to the SWCM using the Euler-centered scheme in time. We shall estimate the error of the proposed SWCM and prove that the scheme is stable and convergent. First, the truncation error of the SWCM is considered. With $\|\cdot\|$ we will indicate the $L^2(a,b)$ norm.

Theorem 3.2. *Suppose* $u(x,t) \in H^s(a,b),\ s \geqslant \frac{5}{2},\ \forall t \in [0,T],\ u(x,t) \in C^4(a,b),\ \forall x \in [a,b]$. *Let* $F(u)$ *be a smooth function. Then the truncation error* R^n *of the SWCM (24) satisfies*

$$\|R^n\| \leqslant O(\tau^2 + 2^{-J(s-2)}).$$

Proof. Let $U^n = (u(x_0,t_n), u(x_1,t_n), \ldots, u(x_{N-1},t_n))$ be the solution of (2). Based on Taylor expanding, the following equations can be obtained,

$$U^{n+1} - 2U^n + U^{n-1} = \tau^2 U_{tt}^n + O(\tau^4),$$
$$U^{n+1} + 2U^n + U^{n-1} = 4U^n + \tau^2 U_{tt}^n + O(\tau^4),$$

and

$$\frac{1}{2}\left(F'\left(\frac{U^{n+1} + U^n}{2}\right) + F'\left(\frac{U^{n-1} + U^n}{2}\right)\right) - F'(U^n) = \tau^2 \cdot \frac{U_{tt}^n}{4} \cdot F''(U^n) + O(\tau^4).$$

Hence, the truncation error of the SWCM (24) goes as

$$\begin{aligned} R^n &= \frac{U^{n+1} - 2U^n + U^{n-1}}{\tau^2} - B_2\left(\frac{U^{n+1} + 2U^n + U^{n-1}}{4}\right) + \frac{1}{2}\left(F'\left(\frac{U^{n+1} + U^n}{2}\right) + F'\left(\frac{U^{n-1} + U^n}{2}\right)\right) \\ &= U_{tt}^n + O(\tau^2) - B_2\left(U^n + \frac{\tau^2}{4}U_{tt}^n + O(\tau^4)\right) + \frac{1}{2}\left(F'\left(\frac{U^{n+1} + U^n}{2}\right) + F'\left(\frac{U^{n-1} + U^n}{2}\right)\right) - \left(U_{tt}^n - U_{xx}^n + F'(U^n)\right) \\ &= U_{xx}^n - B_2 U^n - B_2\left(\frac{\tau^2}{4}U_{tt}^n\right) + \frac{1}{2}\left(F'\left(\frac{U^{n+1} + U^n}{2}\right) + F'\left(\frac{U^{n-1} + U^n}{2}\right)\right) - F'(U^n) + O(\tau^2) \\ &= U_{xx}^n - B_2 U^n - \tau^2\left(\frac{1}{4}B_2 U_{tt}^n\right) + \tau^2\left(\frac{1}{4}U_{tt}^n \cdot F''(U^n)\right) + O(\tau^2). \end{aligned}$$

From Lemma 2.1, we get

$$\left\|u_{xx}^n - \theta_{xx}u^n\right\|_{L^2} \leqslant \|u^n - I_J u^n\|_2 \leqslant C2^{-J(s-2)}\|u^n\|_s,$$

where $\|\cdot\|_s$ denotes the norm of Soblev space $H^s(a,b)$. Notice that

$$\left\|U_{xx}^n - B_2U^n\right\| = \left\{\sum_{m=0}^{N-1} 2^{-J}\cdot\left[u_{xx}^n(x_m) - \theta_{xx}u^n(x_m)\right]^2\right\}^{1/2}$$

is the rectangle quadrature rule approximation to $\left\|u_{xx}^n - \theta_{xx}u^n\right\|_{L^2}$. Therefore, we get the error estimate

$$\|R^n\| \leqslant \left\|U_{xx}^n - B_2U^n\right\| + \tau^2\left\|\frac{1}{4}B_2U_{tt}^n\right\| + \tau^2\left\|\frac{1}{4}U_{tt}^n\cdot F''(U^n)\right\| + O(\tau^2) \leqslant O(2^{-J(s-2)} + \tau^2).$$

This completes the proof. □

Then, the following error estimate of the SWCM is obtained.

Theorem 3.3. *Suppose $u(x,t)$ and $F(u)$ are the same as in Theorem 3.2 . Let U^n and U_J^n be the solutions of (2) and (27), respectively, and $e^n = U^n - U_J^n$. Then the error estimate of the SWCM (24) at time T satisfies*

$$\|e^L\| \leqslant O(\tau^2 + 2^{-J(s-2)}), \quad L = \frac{T}{\tau}.$$

Proof. The truncation error of the SWCM (24) can be written as

$$R^n = \frac{e^{n+1} - 2e^n + e^{n-1}}{\tau^2} - B_2\left(\frac{e^{n+1} + 2e^n + e^{n-1}}{4}\right) + \frac{1}{2}\left(F'\left(U_J^{n+1/2}\right) + F'\left(U_J^{n-1/2}\right)\right) - F'(U^n). \tag{28}$$

Define

$$\delta_t e^{n+1/2} = \frac{e^{n+1} - e^n}{\tau}$$

and make inner product of the both sides of (28) with $\delta_t e^{n+1/2} + \delta_t e^{n-1/2}$, it follows that

$$\begin{aligned}&\frac{1}{\tau}(\|\delta_t e^{n+1/2}\|^2 - \|\delta_t e^{n-1/2}\|^2) + \frac{1}{\tau}(\langle -B_2e^{n+1/2}, e^{n+1/2}\rangle - \langle -B_2e^{n-1/2}, e^{n-1/2}\rangle)\\ &\quad = -\left\langle\frac{1}{2}\left(F'\left(U_J^{n+1/2}\right) + F'\left(U_J^{n-1/2}\right)\right) - F'(U^n), \delta_t e^{n+1/2} + \delta_t e^{n-1/2}\right\rangle + \langle R^n, \delta_t e^{n+1/2} + \delta_t e^{n-1/2}\rangle.\end{aligned}$$

Next, define a discrete function W^n as

$$W^n = \|\delta_t e^{n+1/2}\|^2 + \|e^n\|^2 + \|e^{n+1}\|^2 + \langle -B_2e^{n+1/2}, e^{n+1/2}\rangle.$$

In order to estimate W^n, several inequations are employed here. First, since $F'(U)$ satisfies

$$\left\|F'\left(U_J^{n+1/2}\right) - F'(U^{n+1/2})\right\| = \|F'(U^{n+1/2} - e^{n+1/2}) - F'(U^{n+1/2})\| \leqslant C\|e^{n+1/2}\|,$$

where $C = \max_{x\in[a,b],t\in[0,T]}F'(u(x,t))$, it follows that

$$\begin{aligned}&\left\langle\frac{1}{2}\left(F'\left(U_J^{n+1/2}\right) + F'\left(U_J^{n-1/2}\right)\right) - F'(U^n), \delta_t e^{n+1/2} + \delta_t e^{n-1/2}\right\rangle\\ &\quad \leqslant \frac{1}{2}C(\|e^{n+1/2}\| + \|e^{n-1/2}\|)\|\delta_t e^{n+1/2} + \delta_t e^{n-1/2}\| \leqslant \frac{1}{4}C(\|e^{n+1}\|^2 + 2\|e^n\|^2 + \|e^{n-1}\|^2) + \frac{1}{2}C(\|\delta_t e^{n+1/2}\|^2 + \|\delta_t e^{n-1/2}\|^2).\end{aligned}$$

Then, from Theorem 3.2, the matrix $-B_2$ is symmetric and positive semidefinite, hence

$$\langle -B_2e^{n+1/2}, e^{n+1/2}\rangle \geqslant 0. \tag{29}$$

In addition, notice that

$$\frac{\|e^{n+1}\|^2 - \|e^{n-1}\|^2}{\tau} = \langle e^{n+1} + e^{n-1}, \delta_t e^{n+1/2} + \delta_t e^{n-1/2}\rangle \leqslant \|e^{n+1}\|^2 + \|e^n\|^2 + \|e^{n-1}\|^2 + \|\delta_t e^{n+1/2}\|^2 + \|\delta_t e^{n-1/2}\|^2.$$

Therefore, we have

$$\begin{aligned}\frac{W^n - W^{n-1}}{\tau} &= \frac{\|\delta_t e^{n+1/2}\|^2 - \|\delta_t e^{n-1/2}\|^2}{\tau} + \frac{\langle -B_2e^{n+1/2}, e^{n+1/2}\rangle}{\tau} - \frac{\langle -B_2e^{n-1/2}, e^{n-1/2}\rangle}{\tau} + \frac{\|e^{n+1}\|^2 - \|e^{n-1}\|^2}{\tau}\\ &= \langle R^n, \delta_t e^{n+1/2} + \delta_t e^{n-1/2}\rangle - \left\langle\frac{1}{2}\left(F'\left(U_J^{n+1/2}\right) + F'\left(U_J^{n-1/2}\right)\right) - F'(U^n), \delta_t e^{n+1/2} + \delta_t e^{n-1/2}\right\rangle + \frac{\|e^{n+1}\|^2 - \|e^{n-1}\|^2}{\tau}\\ &\leqslant \|R^n\|^2 + \|\delta_t e^{n+1/2}\|^2 + \|\delta_t e^{n-1/2}\|^2 + \frac{1}{4}C(\|e^{n+1}\|^2 + 2\|e^n\|^2 + \|e^{n-1}\|^2) + \frac{1}{2}C(\|\delta_t e^{n+1/2}\|^2 + \|\delta_t e^{n-1/2}\|^2)\\ &\quad + \|e^{n+1}\|^2 + \|e^n\|^2 + \|e^{n-1}\|^2 + \|\delta_t e^{n+1/2}\|^2 + \|\delta_t e^{n-1/2}\|^2\\ &\leqslant A^n + C_1(W^n + W^{n-1}),\end{aligned}$$

where $C_1 = 2 + \frac{C}{2}$. And the estimate of W^L can be obtained by using Gronwall inequation [30],

$$W^L \leqslant \left(W^0 + \tau \sum_{k=1}^{L} A^k\right) e^{4C_1 T}. \tag{30}$$

Because

$$\|e^0\|^2 = \|R^0\|^2 = 0, \quad \|e^1\|^2 = O(\tau^2 + 2^{-J(s-2)})^2,$$

we have

$$W^0 = O(\tau^2 + 2^{-J(s-2)})^2.$$

In addition, from Theorem 3.2, we have

$$A^k = \|R^n\|^2 = O(\tau^2 + 2^{-J(s-2)})^2.$$

And based on the Gronwall inequation, it follows that

$$W^L = \|\delta_t e^{L+1/2}\|^2 + \|e^L\|^2 + \|e^{L+1}\|^2 + \langle -B_2 e^{L+1/2}, e^{L+1/2}\rangle \leqslant C \cdot O(\tau^2 + 2^{-J(s-2)})^2.$$

Finally, we have obtained the error estimate as

$$\|e^L\| \leqslant O(\tau^2 + 2^{-J(s-2)}).$$

This completes the proof. □

In a similar deductive procedure, a symplectic wavelet collocation method using s-stage Runge–Kutta method for time discretization has $2s$-order in time.

3.2.2. Conservation of discretized Hamiltonian and momentum

3.2.2.1. Discretized Hamiltonian. Assume $F''(u)$ and u_t have uniform bounds both in space and time, then the following error estimate of the Hamiltonian holds.

Theorem 3.4. *Using the symplectic wavelet collocation method (24) , we have*

$$\left|hH_h^L - hH_h^0\right| = O(\tau^2), \quad L = \frac{T}{\tau}.$$

Proof. Suppose (U_J, V_J) is the solution of the symplectic wavelet collocation method (24), and define $H_h^{n+1/2}$ as

$$H_h\left(U_J^{n+1/2}, V_J^{n+1/2}\right) = \left\langle V_J^{n+1/2}, V_J^{n+1/2}\right\rangle + \left\langle F\left(U_J^{n+1/2}\right), \mathbf{1}\right\rangle - \left\langle U_J^{n+1/2}, B_2 U_J^{n+1/2}\right\rangle.$$

Then, by taking inner products of (27) with $\frac{2}{\tau}\left(U_J^{n+1/2} - U_J^{n-1/2}\right)$, we obtain

$$\begin{aligned} hH_h^{n+1/2} - hH_h^{n-1/2} &= -h\left\langle \frac{1}{2}\left(F'\left(U_J^{n+1/2}\right) + F'\left(U_J^{n-1/2}\right)\right), U_J^{n+1/2} - U_J^{n-1/2}\right\rangle + h\left\langle F\left(U_J^{n+1/2}\right) - F\left(U_J^{n-1/2}\right), \mathbf{1}\right\rangle \\ &= h\sum_{m=0}^{N-1}\left[\int_{u_J^{n-1/2}(x_m)}^{u_J^{n+1/2}(x_m)} F'(u_J)du - \frac{1}{2}\left(F'\left(u_J^{n+1/2}(x_m)\right) + F'\left(u_J^{n-1/2}(x_m)\right)\right)\left(u_J^{n+1/2}(x_m) - u_J^{n-1/2}(x_m)\right)\right] \\ &= h\sum_{m=0}^{N-1}\left[-\frac{1}{12}F'''(\tilde{u}_m)\left(u_J^{n+1/2}(x_m) - u_J^{n-1/2}(x_m)\right)^3\right] = h\sum_{m=0}^{N-1}\left[-\frac{1}{12}F'''(\tilde{u}_m)(u_t(x_m, \tilde{t}_m))^3\tau^3\right], \end{aligned}$$

where $\tilde{u}_m \in \left[\min\left(u_J^{n-1/2}(x_m), u_J^{n+1/2}(x_m)\right), \max\left(u_J^{n-1/2}(x_m), u_J^{n+1/2}(x_m)\right)\right]$, and $\tilde{t}_m \in (t^{n-1/2}, t^{n+1/2})$. Thus, the following estimate holds

$$\left|hH_h^{n+1/2} - hH_h^{n-1/2}\right| = \left|h\sum_{m=0}^{N-1}\left[-\frac{1}{12}\cdot F'''(\tilde{u}_m)\cdot(u_t(x_m, \tilde{t}_m))^3\cdot\tau^3\right]\right| \leqslant \left|hC\sum_{m=0}^{N-1}\tau^3\right| \leqslant C\cdot(b-a)\cdot\tau^3,$$

where $C = \max_{x\in[a,b],t\in[0,T]}\left|F_u'''(u(x,t))\cdot(u_t(x,t))^3\right|$.

Therefore,

$$\left|hH_h^L - hH_h^0\right| \leqslant 2\cdot\sum_{n=1}^{L}\left|hH_h^{n+1/2} - hH_h^{n-1/2}\right| \leqslant 2\cdot C\cdot(b-a)\cdot T\cdot\tau^2 = O(\tau^2).$$

This completes the proof. □

3.2.2.2. Discretized momentum. The discrete momentum is $hM_h(U_J, V_J)$ with

$$M_h(U_J, V_J) = -\langle V_J, B_1 U_J \rangle, \tag{31}$$

where B_1 is the wavelet collocation approximation to the first order derivative.

For a symmetric space discretization, the momentum is conserved through the integration for symmetric initial conditions. Although it is not conserved for general initial conditions, it is approximated very well. The details have been discussed in [3]. Now, the results associated with the wavelet collocation space discretization are proposed.

Case 1. Symmetric initial conditions

In this case, the initial value (U_0, V_0) satisfy

$$DU_0 = U_0, \quad DV_0 = V_0,$$

where

$$D = \begin{pmatrix} 0 & 0 & \cdots & 1 \\ \vdots & & \cdot & 0 \\ \vdots & 1 & & \vdots \\ 1 & & \cdots & 0 \end{pmatrix}_{N\times N}.$$

Theorem 3.5. *Assume the initial condition is symmetric, and the wavelet collocation method is employed for space discretization, it happens that*

$$M_h(U_J(t), V_J(t)) = -\langle V_J(t), B_1 U_J(t) \rangle = 0.$$

Proof. As proved in Theorem 3.1, B_2 is a symmetric circulant matrix, we have

$$DB_2 = B_2 D.$$

Then, the solution of (21) is symmetric for any time t, and it satisfies

$$DU_J(t) = U_J(t), \quad t > 0.$$

Consequently, $V_J(t) = \dot{U}_J(t)$ is also symmetric, and

$$DV_J(t) = V_J(t), \quad t > 0.$$

In addition, B_1 is an antisymmetric circulant matrix, thus

$$DB_1 = -B_1 D.$$

Therefore,

$$\langle V_J(t), B_1 U_J(t) \rangle = \langle DV_J(t), DB_1 U_J(t) \rangle = -\langle DV_J(t), B_1 DU_J(t) \rangle = -\langle V_J(t), B_1 U_J(t) \rangle,$$

from which the theorem follows. □

Theorem 3.6. *Under the hypothesis of Theorem 3.5 , the numerical approximation* $\left(U_J^n, V_J^n\right)$ *at* t_n *of system (21) given by symplectic time integrator satisfies*

$$M_h\left(U_J^n, V_J^n\right) = \left\langle V_J^n, B_1 U_J^n \right\rangle = 0.$$

Case 2. General initial conditions

In this case, the continuous momentum does not vanish, but it is well approximated. The following estimate is obtained.

Theorem 3.7. *Suppose* $u(x,t) \in H^s(a,b),\ \forall t \in [0,T]$, *and* $F(u)$ *is a smooth function. Using the wavelet collocation discretization* B_1 *in (19) , it happens that*

$$\frac{d}{dt} h\langle V_J(t), B_1 U_J(t) \rangle \leqslant O(2^{-J(s-1)}).$$

Proof. Since B_1 and $B_2 B_1$ are antisymmetric (proved in Theorem 3.1), we have

$$\langle B_2 U_J, B_1 U_J \rangle = U_J^T B_2 B_1 U_J = \langle U_J, B_2 B_1 U_J \rangle = 0,$$

then

$$\frac{d}{dt}h\langle V_J(t),B_1U_J(t)\rangle = h\langle B_2U_J(t)-F'(U_J(t)),B_1U_J(t)\rangle + \langle V_J(t),B_1V_J(t)\rangle = h\langle B_2U_J(t)-F'(U_J(t)),B_1U_J(t)\rangle$$
$$= h\langle F'(U_J(t)),B_1U_J(t)\rangle.$$

Notice that $h\langle F'(U_J(t)),B_1U_J(t)\rangle$ is the rectangle quadrature rule approximation to $\int_a^b f_J(t)dx$, where

$$f_J(t) = F'(u_J(t))\frac{d}{dx}(F(u_J(t))).$$

As $u_J(t)$ is periodic in $[a,b]$, $\int_a^b f_J(t)dx = 0$. Denote the approximation by $Q_R(f_J(t))$, it follows that

$$Q_R(f_J(t)) = Q_R(I_J(f_J(t))) = \int_a^b I_J(f_J(t))dx = \int_a^b (I_J(f_J(t)) - f_J(t))dx + \int_a^b f_J(t)dx = \int_a^b (I_J(f_J(t)) - f_J(t))dx.$$

Since $u(x,t)\in H^s(a,b)$, $\forall t\in[0,T]$, then, $f_J(t)\in H^{s-1}(a,b)$, $\forall t\in[0,T]$. According to Lemma 2.1, it can be concluded that

$$\int_a^b (I_J(f_J(t)) - f_J(t))dx \leqslant O(2^{-J(s-1)}).$$

Therefore, the theorem is valid since $Q_R(f_J(t)) \leqslant O(2^{-J(s-1)})$. □

4. Symplectic wavelet collocation method for the NLS equation

We briefly consider the NLS equation

$$iu_t + u_{xx} + \beta|u|^2u = 0, \tag{32}$$

where $\beta > 0$ is a constant parameter. Let $u(x,t) = p(x,t) + iq(x,t)$, where $p(x,t)$ and $q(x,t)$ are real functions, the Hamiltonian formulation of (32) is

$$\begin{cases} p_t = -q_{xx} - \beta(p^2+q^2)q, \\ q_t = p_{xx} + \beta(p^2+q^2)p. \end{cases} \tag{33}$$

In this system, the following global quantities are conserved [3]

$$H = \frac{1}{2}\int_{-\infty}^{\infty}\left[p_x^2 + q_x^2 - \frac{\beta}{2}(p^2+q^2)^2\right]dx,$$
$$I_1 = -\frac{1}{2}\int_{-\infty}^{\infty}[p^2+q^2]dx,$$
$$I_2 = \frac{1}{2}\int_{-\infty}^{\infty}[pq_x - qp_x]dx.$$

After wavelet collocation discretization in space, (33) becomes

$$\begin{cases} \frac{d}{dt}p_J(x_m,t) = -(B_2Q_J)_m - \beta(p_J(x_m,t)^2 + q_J(x_m,t)^2)q_J(x_m,t), \\ \frac{d}{dt}q_J(x_m,t) = (B_2P_J)_m + \beta(p_J(x_m,t)^2 + q_J(x_m,t)^2)p_J(x_m,t), \end{cases} \tag{34}$$

where $x_m = a + m/2^J$, $m = 0,1,\ldots,N-1$, $N = (b-a)\cdot 2^J$ and $P_J = (p_J(x_0,t),p_J(x_1,t),\ldots,p_J(x_{N-1},t))^T$, $Q_J = (q_J(x_0,t),q_J(x_1,t),\ldots,q_J(x_{N-1},t))^T$. Discretizing this system by the Euler-centered scheme in time, we obtain the standard symplectic wavelet collocation method for the NLS equation:

$$\begin{cases} P_J^{n+1} = P_J^n - \tau\left(B_2\cdot Q_J^{n+1/2} + \beta\left(\left(P_J^{n+1/2}\right)^{.2} + \left(Q_J^{n+1/2}\right)^{.2}\right)\cdot Q_J^{n+1/2}\right), \\ Q_J^{n+1} = Q_J^n + \tau\left(B_2\cdot P_J^{n+1/2} + \beta\left(\left(Q_J^{n+1/2}\right)^{.2} + \left(P_J^{n+1/2}\right)^{.2}\right)\cdot P_J^{n+1/2}\right), \end{cases} \tag{35}$$

where

$$P_J^{n+1/2} = \frac{P_J^n + P_J^{n+1}}{2}, \quad \left(P_J^{n+1/2}\right)^{.2} = \left(P_J^{n+1/2}\right)^T\left(P_J^{n+1/2}\right).$$

The discrete Hamiltonian is

$$H_h(P_J,Q_J) = -\frac{1}{2}\left[\langle Q_J, B_2Q_J\rangle + \langle P_J, B_2P_J\rangle + \frac{\beta}{2}\langle (P_J{}^{.2} + Q_J{}^{.2})^{.2}, \mathbf{1}\rangle\right].$$

According to the results in [3], the following results can be easily obtained for the special properties of the space differentiation matrix:

(R1) For wavelet collocation method, B_2 is symmetric,

$$I_{1,h} = -\frac{1}{2}[\langle P_J, P_J\rangle + \langle Q_J, Q_J\rangle]$$

is a first integral of semi-discretization Hamiltonian system (34).

(R2) As B_2 is symmetric, by using symplectic Runge–Kutta method for time discretization, it happens that

$$hI_{1,h}\left(P_J^n, Q_J^n\right) - hI_{1,h}\left(P_J^0, Q_J^0\right) = 0, \quad n > 0.$$

What's more, the discretization of the continuous invariant I_2 is

$$I_{2,h} = \frac{1}{2}[\langle P_J, B_1 Q_J\rangle - \langle Q_J, B_1 P_J\rangle]. \tag{36}$$

Then, exactly in the same way as in Theorem 3.5, the following result holds.

(R3) Assume the initial condition is symmetric, when the wavelet collocation method is taken for space discretization, it happens that

$$I_{2,h}(P_J, Q_J) = \frac{1}{2}[\langle P_J, B_1 Q_J\rangle - \langle Q_J, B_1 P_J\rangle] = 0. \tag{37}$$

Also after full discretization, similar to Theorem 3.6, we can gain the following result.

(R4) Under hypothesis of (R3), the numerical approximation $\left(P_J^n, Q_J^n\right)$ at t_n of system (34) given by symplectic time integrator satisfies

$$I_{2,h}\left(P_J^n, Q_J^n\right) = 0.$$

In the following section, various numerical experiments will be conducted to substantiate the above theoretical analysis.

5. Numerical investigation for the NLW and NLS equations

In this section, numerical experiments are presented for the NLW and NLS equations to illustrate the following numerical characters of the proposed SWCM: (1) high order of accuracy; (2) long time simulation; (3) conservation of invariants; (4) singularity capturing.

For convenience, the SWCM taking B_2 based on the autocorrelation function of Daubechies scaling function DM is called SWCM with ADM (abbr. SWCM-ADM).

5.1. Numerical simulation for the NLW equation

To gain insight into the performance of the proposed SWCM (24) for the NLW equation (2), the following numerical experiments are performed. To show the advantage of the proposed method, a singular linear problem is considered in Example 5.1. Space and time accuracy of the SWCM-AD10 is tested and SWCM is compared with other methods with different spatial discretization. To illustrate the properties of the SWCM in long time simulating and invariants conserving, long time simulation are made for the NLW equation and the errors in invariants are given in Examples 5.2 and 5.3. In addition, symmetric and nonsymmetric initial conditions are simulated to confirm the results about conservation of invariants and the SWCM-AD10 is used for solving those problems.

Example 5.1. An accuracy test is taken by considering the linear wave equation

$$u_{tt} = u_{xx} \tag{38}$$

with symmetric initial conditions

$$u(x,0) = f(x) = \exp(-3200x^2), \quad v(x,0) = 0. \tag{39}$$

This problem is singular and the true solution is

$$u(x,t) = \frac{1}{2}[f(x+t) + f(x-t)].$$

First, the problem is considered in the spatial interval $[-1,1]$ till time $T = 0.6$ for accuracy test. Fixed-point iteration method with tolerance 10^{-30} is used to solve (24). The space and time accuracy of the SWCM (24) with AD10 are tested.

The L^2 and L^∞ errors, as well as the numerical order of accuracy, are contained in Tables 1 and 2. As expected, the errors decrease at an exponential rate with respect to the space grid number N. For example, the L^∞ error decreases from 5.1928×10^{-2} to 1.0387×10^{-6} when N changes from 128 to 1024. In addition, the scheme has second-order of accuracy in time, which agrees with Theorem 3.3.

For the purpose of numerical comparisons, we consider a symplectic Fourier pseudospectral method (abbr. SFPSM), which uses the pseudospectral scheme in space and the Euler-centered scheme in time, and a symplectic finite difference method (abbr. SFDM), which uses the fourth-order central difference scheme in space and the Euler-centered scheme in time. SWCM is compared with those methods from spatial accuracy and CPU time aspects. Table 3 shows the numerical errors and CPU time of SWCM (with different ADM), SFPSM and SFDM. SWCM is of higher order of accuracy than SFDM. The errors of SWCM decrease in an exponential rate in space for each ADM and the decreasing rate is increasing when M becomes larger. In addition, for a given grid number N, the errors of SWCM will approximate to those of SFPSM when M becomes larger. Moreover, SWCM-AD20 with $N = 512$ takes less CPU time than SFPSM with $N = 256$, which tell us that SWCM is more efficient than SFPSM to obtain similar approximation for this singular problem. Furthermore, the errors of SFPSM increase when N changes from 256 to 512, while the errors of SWCM are still decrease rapidly. These numerical results seems to reveal that SWCM takes a good balance of accuracy (SFPSM) and efficiency (SFDM).

Second, the problem is solved in $[-1, 1]$ till $T = 100$ with periodic boundary condition by using SWCM-AD20. As shown in Fig. 2, the problem is well simulated, the two wave forms of smaller amplitudes travel in opposite directions and meet at $x = \pm 1$ or $x = 0$. This result is obtained by taking $\tau = 0.0001$ and $N = 512$.

Example 5.2. Consider the kink–antikink solution of the sine-Gordon equation [5]

$$u_{tt} = u_{xx} - \sin(u) \tag{40}$$

with symmetric initial conditions

$$u_0(x) = 0, \quad v_0(x) = 4\gamma \operatorname{sech}(\gamma x). \tag{41}$$

Table 1
Space accuracy test of the SWCM-AD10 for (38) with initial condition (39) ($\tau = 0.0000002$).

J	N	Error		Order	
		L^∞	L^2	L^∞	L^2
6	128	0.1542	5.1928e−2	–	–
7	256	3.3477e−2	9.7851e−3	2.2036	2.4079
8	512	9.0917e−4	1.8943e−4	5.2025	5.6908
9	1024	5.4464e−6	1.0387e−6	7.3831	7.5107

Table 2
Time accuracy test of the SWCM-AD10 for (38) with initial condition (39) ($J = 9,\ N = 1024$).

τ	Error		Order	
	L^∞	L^2	L^∞	L^2
0.0004	2.8313e−3	5.8908e−4	–	–
0.0002	7.0068e−4	1.4702e−4	2.0146	2.0025
0.0001	1.7273e−4	3.6407e−5	2.0202	2.0137
0.00005	4.0642e−5	8.7782e−6	2.0875	2.0522

Table 3
Comparison of the SWCM, SFPSM and SFDM for (38) with initial condition (39) ($\tau = 0.0000002$).

	SWCM-AD10	SWCM-AD20	SWCM-AD30	SFPSM	SFDM
$N = 128$					
L_∞ errors	0.15	5.70E−02	4.31E−02	6.19E−03	0.18
L_2 errors	5.19E−02	2.28E−02	1.63E−02	3.88E−03	5.73E−02
CPU (s)	442.81	836.03	1230.42	2296.58	177.77
$N = 256$					
L_∞ errors	3.35E−02	2.59E−03	5.33E−04	8.78E−06	6.86E−02
L_2 errors	9.79E−03	6.87E−04	1.62E−04	9.41E−06	1.54E−02
CPU (s)	889.14	1734.31	2526.36	8886.75	358.19
$N = 512$					
L_∞ errors	9.09E−04	7.85E−07	5.93E−09	3.46E−05	6.99E−03
L_2 errors	1.89E−04	1.53E−07	1.27E−09	3.77E−05	1.38E−03
CPU (s)	1988.19	3896.39	6173.52	*215981.06*	760.03

Here $\gamma = 20$ is taken. These initial conditions correspond to two-soliton waves moving with speed $c = \pm 1$ in space and the waves have large spatial gradients. This problem is solved in $[-30, 30]$ till time $T = 200$ by SWCM-AD10 with $\tau = 0.0005$ and $N = 3840$. Fixed-point iteration method with tolerance 10^{-10} is used and CPU time is about 2776 s. As shown in Fig. 3, the

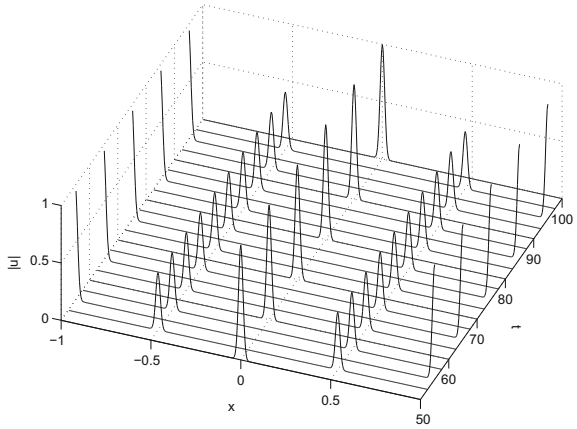

Fig. 2. The wave propagation of (38) with initial condition (39), using SWCM-AD20 ($\tau = 0.0001,\ N = 512$).

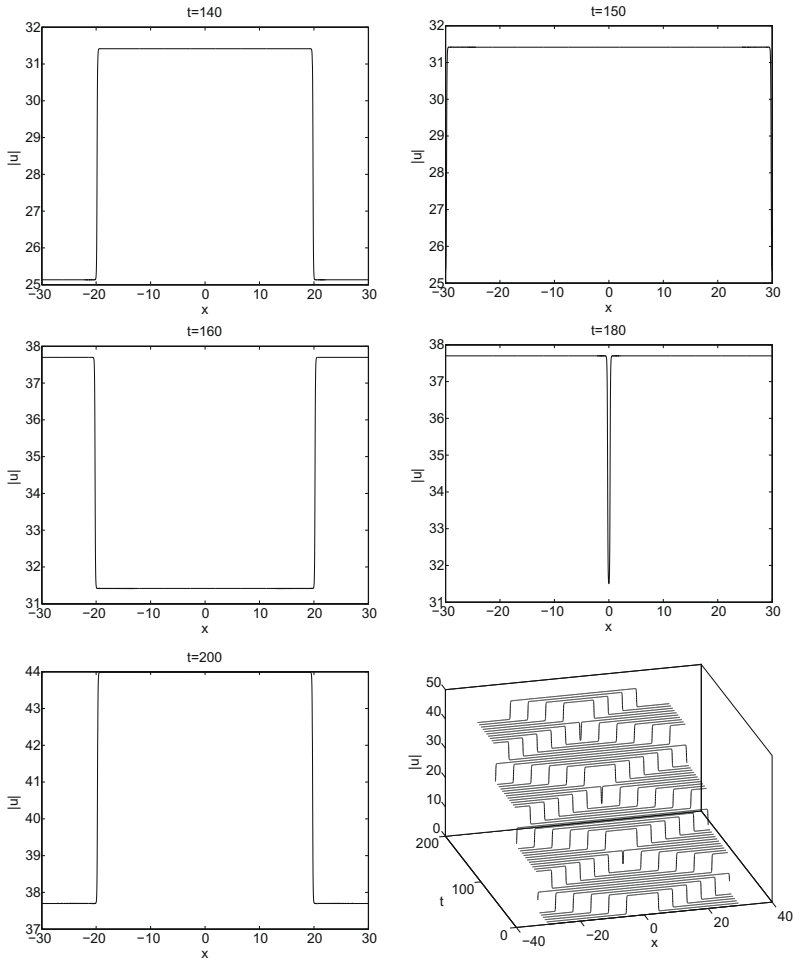

Fig. 3. Waveforms at $t = 140, 150, 160, 180, 200$ and the wave propagation of (40) with initial condition (41) over time interval [0,200], using SWCM-AD10 ($\tau = 0.0005,\ N = 3840$).

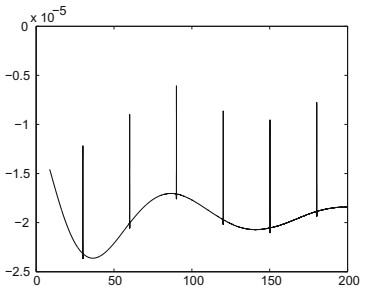

wave propagation is well simulated by the proposed method. In addition, Fig. 4 shows the variation of the errors in Hamiltonian and momentum in the time interval [0,200]. The error in momentum is less than 4.0×10^{-9}, which is negligible. While the error in Hamiltonian is less than 2.5×10^{-5}. And the pronounced spikes in the error of Hamiltonian correspond to the two kinks meet at $x = \pm 30$ or $x = 0$.

Example 5.3. Consider the nonlinear wave equation (1) with

$$F(u) = 0.1u^4 \tag{42}$$

and nonsymmetric initial conditions

$$u_0(x) = \frac{5}{2}e^{\frac{\cos x}{5}} - \frac{5}{2}, \quad v_0(x) = e^{\frac{\sin x}{5}} - \frac{5}{2}, \quad x \in [0, 2\pi]. \tag{43}$$

By taking a coordinate transform $x = \pi\xi$, Eq. (1) can be transformed into

$$u_{tt} = \frac{1}{\pi^2}u_{\xi\xi} - F'(u), \quad \xi \in [0, 2].$$

Then, the problem is solved till time $T = 200$ by SWCM-AD10 with $\tau = 0.002$ and $N = 64$. Fig. 5 shows the variation of the errors in Hamiltonian and momentum in the time interval [0,200]. The error in Hamiltonian is less than 7.05×10^{-6}, while the error in momentum is less than 4.65×10^{-13}.

Table 4 shows the L^∞ errors of Hamiltonian and momentum, which mean the maximum errors in the time interval. For this nonsymmetric initial conditions, the error in momentum depends only on the space step h and decreases exponentially in space, which agrees with Theorem 3.7; while the error in Hamiltonian depends only on the chosen time-step τ and is second-order in τ, which agrees with Theorem 3.4.

The above numerical simulations show that the proposed SWCM not only has high order of accuracy but also has good properties in long time simulation and conservation of invariants. In the following subsection, we will present its generalization to the NLS equation, which has some more singular and complex problems being difficult to simulate.

5.2. Numerical simulation for the NLS equation

In this subsection, one soliton solution, bound state solution and homoclinic structure of the NLS equation are simulated in Examples 5.4–5.6. In Example 5.4, space and time accuracy of the SWCM-AD10 is tested and SWCM is also compared with SFPSM and SFDM as that of the NLW equation. And for this nonsymmetric initial conditions, long time simulation is made and how the invariant I_2 changes according to the space step is also investigated. While in Examples 5.5 and 5.6, some more singular and complex examples with symmetric initial conditions are proposed to confirm the results (R3) and (R4) and to show the good-performance of the method in capturing singularity and preserving the spatial symmetry of solutions. Figures about wave propagation and errors in invariants are given for each example. The errors in the three invariant quantities are measured by the following way

$$h(H_h(P^n, Q^n) - H_h(P^0, Q^0)),$$
$$h(I_{1,h}(P^n, Q^n) - I_{1,h}(P^0, Q^0)),$$
$$h(I_{2,h}(P^n, Q^n) - I_{2,h}(P^0, Q^0)).$$

Unless the contrary is stated, the standard value for the nonlinear constant in (33) is $\beta = 2$.

Example 5.4. An accuracy test is taken for the NLS equation (32) with the one soliton solution [29]

$$u(x,t) = \operatorname{sech}(x - 4t)exp\left(2i\left(cx - \frac{3}{2}t\right)\right), \tag{44}$$

where $c = 1.0$.

First, the problem is considered in $[-50, 50]$ till time $T = 1$ for accuracy test. Fixed-point iteration method with tolerance 10^{-30} is used to solve (35). The space accuracy of the SWCM (35) with AD10 is tested, The L^2 and L^∞ errors and the numerical order of accuracy are given in Tables 5 and 6. Notice that both errors decrease very quickly when the space grid number N becomes larger. As shown in Table 5, the numerical orders measured by the L^∞ error are 2.0951, 5.3489 and 7.0731, which means that the error decays at an exponential rate with respect to the space grid number N. So does the L^2 error.

As shown in Tables 7 and 8, the errors of SWCM decrease in an exponential rate for each ADM and the decreasing rate is increasing when M becomes larger. SWCM is of higher order of accuracy than SFDM. In addition, SWCM-AD30 seems to be as accurate as SFPSM, but taking less CPU time than SFPSM. Moreover, the errors of SWCM are smaller than those of SFPSM when $N = 800$. These numerical results tell us again that SWCM takes a good balance of accuracy (SFPSM) and efficiency (SFDM).

Second, the problem is solved in $[-30, 220]$ till time $T = 50$ by the SWCM-AD10 to test the property of long time simulation. Time evolution of the soliton propagation can be found in Fig. 6, which is obtained by taking $\tau = 0.001$ and $N = 1000$. Notice that the motion of the soliton is simulated very well. The variation of the errors in invariants are displayed

Table 5
Space accuracy test of the SWCM (35) for (32) with AD10 and initial condition (44), the real part ($\tau = 0.000001$).

J	N	Error		Order	
		L^∞	L^2	L^∞	L^2
0	100	0.6477	0.9406	–	–
1	200	0.1516	0.1877	2.0951	2.3252
2	400	3.7199E−03	4.2198E−03	5.3489	5.4751
3	800	2.7625E−05	2.6653E−05	7.0731	7.3067

Table 6
Space accuracy test of the SWCM (35) for (32) with AD10 and initial condition (44), the imaginary part ($\tau = 0.000001$).

J	N	Error		Order	
		L^∞	L^2	L^∞	L^2
0	100	0.6252	0.9801	–	–
1	200	0.1313	0.1927	2.2515	2.3466
2	400	3.3710E−03	4.3684E−03	5.2835	5.4631
3	800	2.2118E−05	2.7465E−05	7.2518	7.3134

Table 7
Comparison of the SWCM, SFPSM and SFDM for (32) with initial condition (44), the real part ($\tau = 0.000001$).

	SWCM-AD10	SWCM-AD20	SWCM-AD30	SFPSM	SFDM
$N = 100$					
L_∞ errors	0.65	0.35	0.29	0.22	0.56
L_2 errors	0.94	*0.48*	0.41	0.37	0.95
CPU (s)	244.00	478.63	700.64	1091.38	89.02
$N = 200$					
L_∞ errors	0.15	1.47E−02	4.08E−03	2.68E−03	0.21
L_2 errors	0.19	1.86E−02	6.89E−03	6.53E−03	0.28
CPU (s)	507.36	1000.61	1545.64	5154.53	178.39
$N = 400$					
L_∞ errors	3.72E−03	1.59E−05	1.17E−06	1.41E−08	1.73E−02
L_2 errors	4.22E−03	1.57E−05	1.71E−06	3.01E−08	1.88E−02
CPU (s)	1100.80	2080.25	3122.78	28074.52	359.66
$N = 800$					
L_∞ errors	2.76E−05	1.38E−09	4.42E−11	2.59E−10	1.11E−03
L_2 errors	2.67E−05	1.17E−09	4.65E−11	2.58E−10	1.21E−03
CPU (s)	2465.27	4582.67	6588.33	151,417.86	765.78

Table 8
Comparison of the SWCM-ADM, SFPSM and SFDM for (32) with initial condition (44), the imaginary part ($\tau = 0.000001$).

	SWCM-AD10	SWCM-AD20	SWCM-AD30	SFPSM	SFDM
$N = 100$					
L_∞ errors	0.63	0.31	0.26	0.22	0.55
L_2 errors	0.98	*0.59*	0.51	0.44	0.93
$N = 200$					
L_∞ errors	0.13	1.38E−02	4.47E−03	2.56E−03	0.33
L_2 errors	0.19	1.94E−02	7.43E−03	6.47E−03	0.32
$N = 400$					
L_∞ errors	3.37E−03	1.49E−05	1.57E−06	2.08E−08	1.52E−02
L_2 errors	4.37E−03	1.57E−05	1.72E−06	3.03E−08	1.95E−02
$N = 800$					
L_∞ errors	2.21E−05	1.36E−09	4.05E−11	2.08E−10	1.00E−03
L_2 errors	2.75E−05	1.18E−09	4.66E−11	2.40E−10	1.26E−03

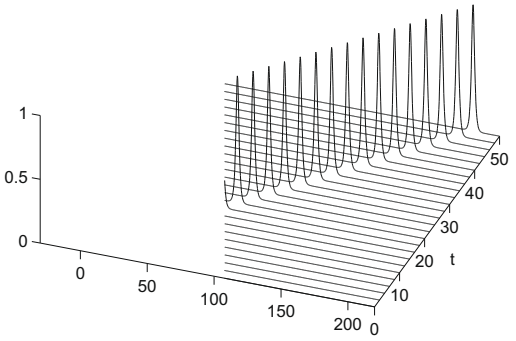

in Fig. 7. We can see the error in Hamiltonian has a bound of 5.90×10^{-8} while the error in I_1 is less than 1.15×10^{-12} and so is negligible. Though the bound of the error in I_2 is 9.67×10^{-7}, it will reduce to 1.04×10^{-11} when N becomes larger according to Table 9.

Third, to see the proposed method in approximating invariants for this nonsymmetric initial conditions, the L^∞ errors of invariants are given in Table 9. The error in I_1 is negligible, which agrees with the result (R2). While the error in I_2 mainly depends on the space step h and decays at an exponential rate. The error in Hamiltonian also decreases exponentially in space and is second-order in τ.

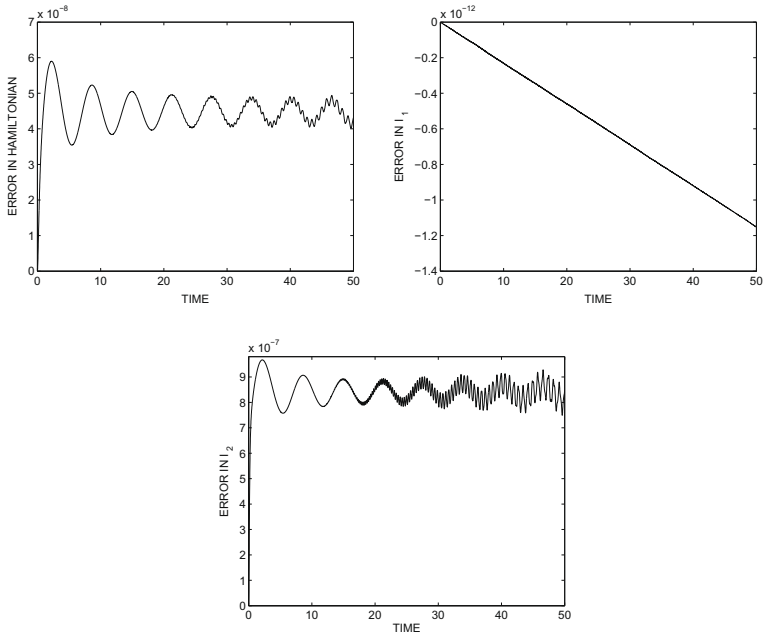

Fig. 7. The variation of the errors in Hamiltonian, I_1 and I_2 ($\tau = 0.001,\ N = 1000$).

Table 9
The errors in invariants of SWCM-AD10 for (32) with initial condition (44) ($T = 50$).

Hamiltonian/I_1/I_2	$\tau = 0.002$	$\tau = 0.001$
$N = 500$	7.46E−06/7.05E−13/4.10E−03	1.87E−06/7.42E−13/4.10E−03
$N = 1000$	2.34E−07/1.16E−12/9.62E−07	5.90E−08/1.15E−12/9.67E−07
$N = 2000$	6.80E−10/1.76E−12/7.19E−12	2.47E−10/1.76E−12/1.04E−11

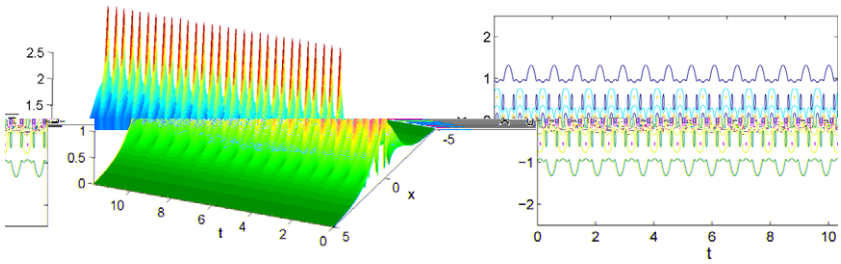

Fig. 8. The nonlinear wave propagation of (32) with initial condition (45), using SWCM-AD10 ($\tau = 0.0001,\ N = 960$).

Example 5.5. We discuss the bound state solution of (32) with the symmetric initial condition [29,32]

$$u(x,0) = \operatorname{sech}(x). \tag{45}$$

It will produce a bound state of K solitons when $\beta = 2 \cdot K^2$. As for $K \geqslant 3$, the solutions are difficult to resolve because of large spatial and temporal gradients in the solutions.

First, for the case $\beta = 2 \cdot 3^2$, the problem is solved in $[-15, 15]$ till time $T = 60$ by SWCM-AD10 with $\tau = 0.0001$ and $N = 960$. In Fig. 8, time evolution of the solution is shown over $t \in [0, 11.8]$, and the corresponding contour picture is also given. As shown in the figure, the proposed method exhibits high resolution in capturing singularities. As can be seen in Fig. 9, the errors in I_1 and I_2 are negligible, which agree with the results (R2) and (R4). The error in total energy is bounded, and the pronounced spikes correspond to the "hill peaks" in the solutions, where the spatial gradients are very high.

Second, for the case $\beta = 2 \cdot 5^2$, we use SWCM-AD30 to solve the problem in $[-15, 15]$ till time $T = 11.8$ with $\tau = 0.00002$ and $N = 960$. The problem has a periodic solution with period of $L \approx 0.7854$, so 15 periods are contained in the time interval $[0, 11.8]$. Fig. 10 shows the approximate solution in the fifteenth period, the evolution of the solution over $t \in [0, 11.8]$ and the

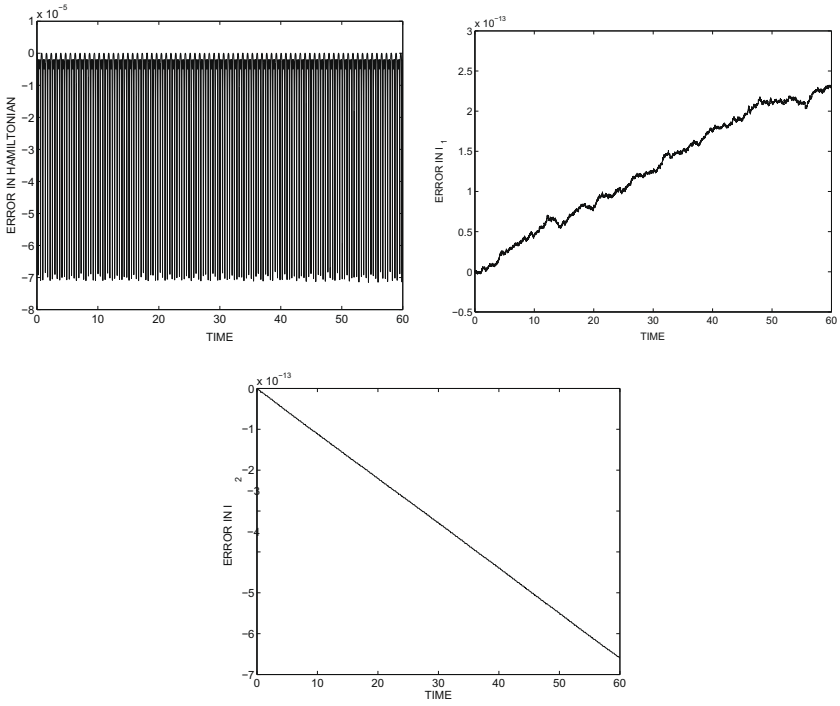

Fig. 9. The variation of the errors in Hamiltonian, I_1 and I_2 ($\tau = 0.0001,\ N = 960$).

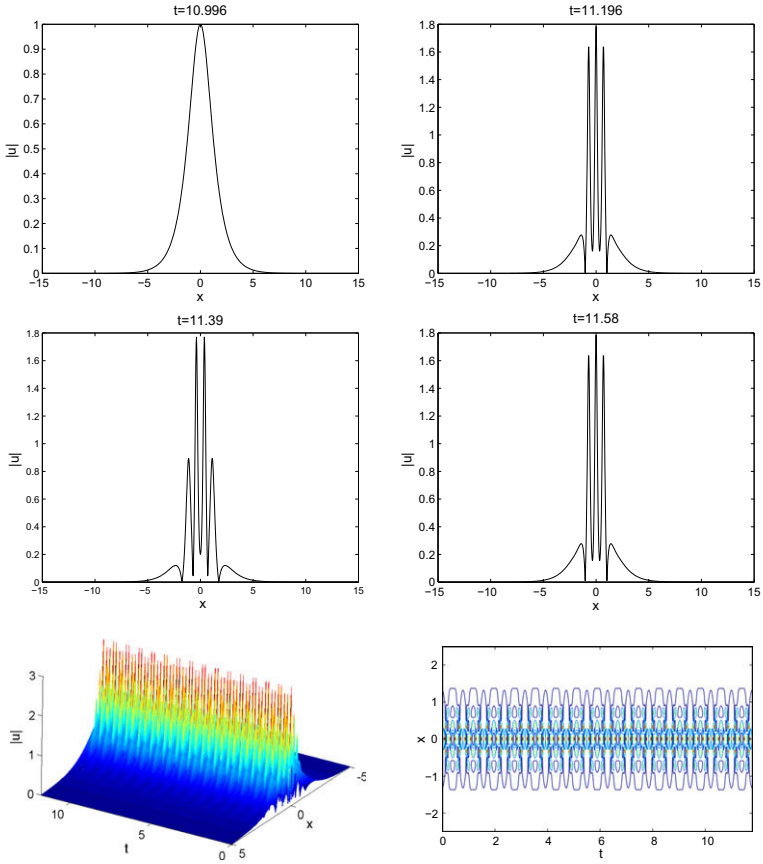

Fig. 10. The nonlinear wave propagation of (32) with initial condition (45), using SWCM-AD30 ($\tau = 0.00002,\ N = 960$).

corresponding contour picture. The proposed method simulates the evolution of the five-soliton bound state solution very well.

Example 5.6. In this example we show the homoclinic structure of (32) with the following periodic initial condition

$$u(x,0) = A[1 + 0.05\cos(\mu x)], \quad x \in [-L/2, L/2], \tag{46}$$

where $\mu = 2\pi/L$ and $L = 4\sqrt{2}\pi$. This initial condition is in the vicinity of the homoclinic structure associated with the NLS equation, which makes it difficult to simulate the solution. The parameter A is used to change the complexity of the homoclinic structure [2,4,24].

By taking a coordinate transform $x = \sqrt{2}\pi\xi$, the problem (32) is equivalent to

$$iu_t + \frac{1}{2\pi^2}u_{\xi\xi} + \beta|u|^2 u = 0, \quad \xi \in [-2, 2].$$

Firstly, we set $A = 0.5$. The problem is solved till $T = 200$ by SWCM-AD10 with $\tau = 0.0002$ and $N = 128$. Time evolution of the waveforms $u(x,t)$ and the corresponding density picture are shown in Fig. 11. It is indicated that the proposed method has high spatial resolution and is stable even after long time simulation. What's more, as shown in Fig. 12, the errors in I_1 and I_2 are negligible, which agree with the results (R2) and (R4). The error in Hamiltonian is bounded, and the pronounced spikes appear in the error of Hamiltonian when the large values appear in the waveforms.

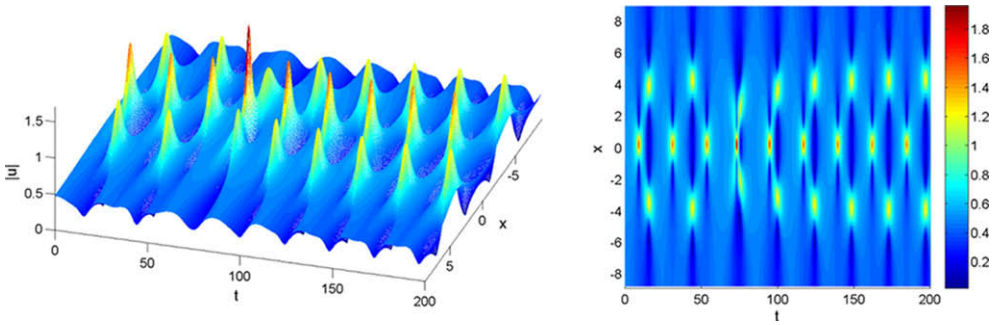

Fig. 11. The nonlinear wave propagation of (32) with initial condition (46), using SWCM-AD10 ($\tau = 0.0002,\ N = 128$).

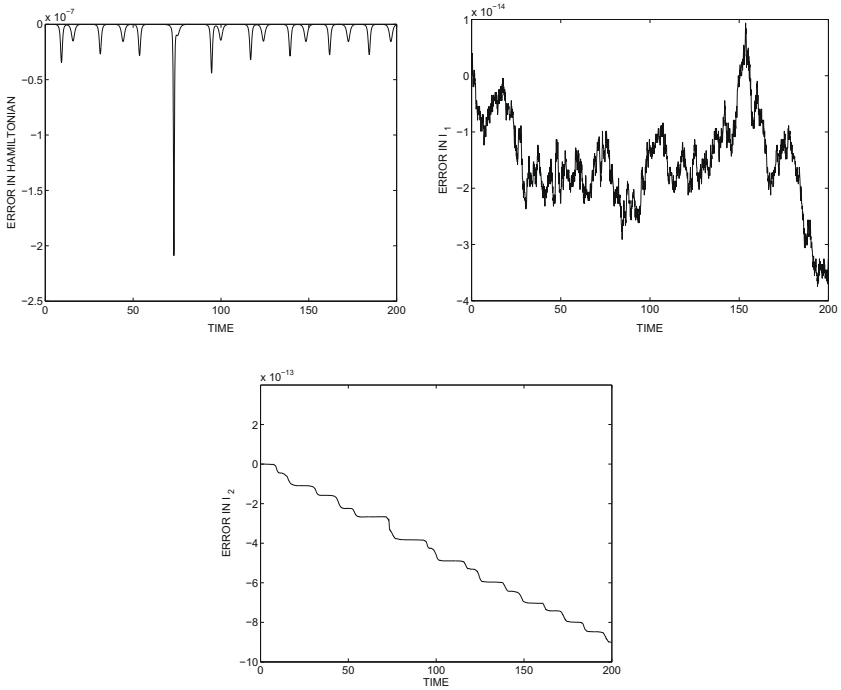

Fig. 12. The variation of the errors in Hamiltonian, I_1 and I_2 ($\tau = 0.0002,\ N = 128$).

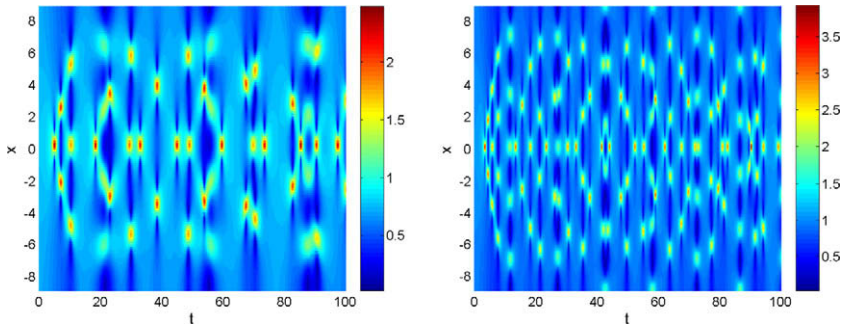

Fig. 13. The nonlinear wave propagation of (32) with initial condition (46), using SWCM-AD10, the left plot: $A = 0.75$, the right plot: $A = 1.0$ ($\tau = 0.0001,\ N = 512$).

Secondly, we increase A to $A = 0.75$ and then to $A = 1.0$, thereby increasing the complexity of the homoclinic structure. The SWCM-AD10 with $\tau = 0.0001$ and $N = 512$ is used. We show the results in the form of density plots. For case $A = 0.75$, which is shown in the left plot in Fig. 13, the spatial symmetry is well preserved and no instability occurs. In addition, the result obtained here is similar with the result obtained by the Fourier pseudospectral scheme and symplectic fourth-order split-step scheme in [2], which use $N = 512$ and $\tau = 0.001$. For case $A = 1.0$, the right plot in Fig. 13 shows the complex structure. Again, the spatial symmetry is preserved and no instability occurs.

The above numerical experiments demonstrate the capability of the proposed method in capturing singularities and conserving invariant quantities. Firstly, the error in Hamiltonian is bounded and depends mainly on the time-step. Secondly, I_1 is conserved exactly no matter the initial condition is symmetric or not, which corresponds to the result (R2). Furthermore, the error in I_2 is negligible for the symmetric initial condition, which agrees quite well with the result (R4). While the error in I_2 is always bounded for nonsymmetric initial condition and diminishes quickly by halving the space step.

6. Conclusions and perspectives

In this paper, symplectic wavelet collocation method is proposed and tested for the NLW and NLS equations. The method is based on the autocorrelation function of compactly supported Daubechies scaling functions. Due to the properties of the basic functions, the space differentiation matrix has many attractive properties which can explain good-performance of the method. The space differentiation matrix is a sparse circulant matrix with limited-bandwidth and so it costs less computational effort. The analytical and numerical results both show that the method has high order of accuracy in space and can capture singularity efficiently, and the discrete invariant quantities can be preserved very well during long-time computation. The proposed method can be generalized to solve any second-order systems with even-order spatial derivatives, and can be also applied to discrete multi-symplectic PDEs. Moreover, by introducing some kind of adaptive procedure, symplectic adaptive wavelet collocation method can be generalized by using the autocorrelation function θ at different scales at the same time.

Acknowledgments

We thank the anonymous referees for useful suggestions. This work was partially supported by the Natural Science Foundation of China (Grant Nos. 10471145, 10971226, 10672143 and 10872037), Singapore AcRF RG59/08 M52110092 and Singapore NRF 2007IDM IDM002-010.

References

[1] A. Latto, H.L. Resnikoff, E. Tenenbaum, The evaluation of connection coefficients of compactly supported wavelets, in: Proceedings of the French-USA Workshop on Wavelets and Turbulence, Springer-Verlag, New York, 1991.
[2] B.M. Herbst, F. Varadi, M.J. Ablowitz, Symplectic methods for the nonlinear Schrödinger equation, Math. Comput. Simul. 37 (1994) 353–369.
[3] B. Cano, Conserved quantities of some Hamiltonian wave equations after full discretization, Numer. Math. 103 (2006) 197–223.
[4] C.M. Schober, Symplectic integrators for Ablowitz–Ladik discrete nonlinear Schrödinger equation, Phys. Lett. A 259 (1999) 140–151.
[5] C.M. Schober, T.H. Wlodarczyk, Dispersive properties of multisymplectic integrators, J. Comput. Phys. 227 (2008) 5090–5104.
[6] D.B. Duncan, Symplectic finite difference approximations of the nonlinear Klein–Gordon equation, SIAM J. Numer. Anal. 34 (1997) 1742–1760.
[7] E. Hairer, Ch. Lubich, G. Wanner, Geometric Numerical Integration: Structure-Preserving Algorithms for Ordinary Differential Equations, Springer, Berlin, 2002.
[8] G. Beylkin, On the representation of operators in bases of compactly supported wavelets, SIAM J. Numer. Anal. 6 (6) (1992) 1716–1740.
[9] N. Saito, G. Beylkin, Multiresolution representations using the autocorrelation of compactly wavelets, IEEE Trans. Sig. Proc. 41 (1993) 3584–3590.
[10] I. Daubechies, Ten Lectures on Wavelets, SIAM, 1992.
[11] J.W. Ma, H.Z. Yang, Multiresolution symplectic scheme for wave propagation in complex media, Appl. Math. Mech. 25 (5) (2004) 573–579.
[12] J.W. Ma, An exploration of multiresolution symplectic scheme for wave propagation using second-generation wavelets, Phys. Lett. A 328 (2004) 36–46.
[13] J.M. Sanz-Serna, M.P. Calvo, Numerical Hamiltonian Problems, Chapman & Hall, London, 1994.

[14] J.B. Chen, Symplectic and multisymplectic Fourier pseudospectral discretizations for the Klein–Gordon equation, Lett. Math. Phys. 75 (2006) 293–305.
[15] K. Feng, On difference schemes and symplectic geometry, in: K. Feng (Ed.), Proceedings of the 1984 Beijing Symposium on Differential Geometry and Differential Equations, Science Press, Beijing, 1985, pp. 42–58.
[16] K. Feng, H.M. Wu, M.Z. Qin, D.L. Wang, Construction of canonical difference schemes for Hamiltonian formalism via generating functions, J. Comput. Math. 7 (1) (1989) 71–96.
[17] L. Qiao, Eight Lectures on Matrix Theory, Shanghai Science and Technology Press, 1988. pp. 47–48.
[18] L.H. Kong, R.X. Liu, X. H Zheng, A survey on symplectic and multi-symplectic algorithms, Appl. Math. Comput. 186 (2007) 670–684.
[19] M. Holmström, J. Waldén, Adaptive wavelet methods for hyperbolic PDEs, J. Sci. Comput. 13 (1) (1998) 19–49.
[20] O.V. Vasilyev, S. Paolucci, M. Sen, A multilevel wavelet collocation method for solving partial differential equations in a finite domain, J. Comput. Phys. 120 (1995) 33–47.
[21] O.V. Vasilyev, S. Paolucci, A fast adaptive wavelet collocation algorithm for multidimensional PDEs, J. Comput. Phys. 138 (1997) 16–56.
[22] O.V. Vasilyev, N.K.-R. Kevlahan, An adaptive multilevel wavelet collocation method for elliptic problems, J. Comput. Phys. 206 (2005) 412–431.
[23] P.J. Channell, J.C. Scovel, Symplectic integration of Hamiltonian systems, Nonlinearity 3 (2) (1990) 231–259.
[24] R.I. McLachlan, Symplectic integration of Hamiltonian wave equations, Numer. Math. 66 (1994) 465–492.
[25] S. Bertoluzza, G. Naldi, A wavelet collocation method for the numerical solution of partial differential equations, Appl. Comput. Harmon. Anal. 3 (1) (1996) 1–9.
[26] S. Reich, Multi-symplectic Runge–Kutta collocation methods for Hamiltonian wave equations, J. Comput. Phys. 157 (2000) 473–499.
[27] T.J. Bridges, S. Reich, Multi-symplectic integrators: numerical schemes for Hamiltonian PDEs that conserve symplecticity, Phys. Lett. A 284 (2001) 184–193.
[28] T.J. Bridges, S. Reich, Numerical methods for Hamiltonian PDEs, J. Phys. A: Math. Gen. 39 (2006) 5287–5320.
[29] Y. Xu, C.W. Shu, Local discontinuous Galerkin methods for nonlinear Schrödinger equations, J. Comput. Phys. 205 (2005) 72–97.
[30] Y.L. Zhou, Application of Discrete Functional Analysis to the Finite Difference Method, International Academic Publishers, Beijing, 1990.
[31] Y.F. Tang, Formal energy of symplectic scheme for Hamiltonian systems and its applications (1), Comput. Math. Appl. 27 (7) (1994) 31–39.
[32] Y.F. Tang, J.W. Cao, X.T. Liu, Y.C. Sun, Symplectic methods for the Ablowitz–Ladik discrete nonlinear Schrödinger equation, J. Phys. A: Math. Theor. 40 (2007) 2425–2437.
[33] L. Zhen, Y.Q. Bai, Q.S. Li, K. Wu, Symplectic and multi-symplectic schemes with the simple finite element method, Phys. Lett. A 314 (2003) 443–455.